Nanoscale

Accepted Manuscript

This article can be cited before page numbers have been issued, to do this please use: P. K. K. Roy, R. K. Ulaganathan, C. M. Raghavan, S. M. Mhatre , H. Lin, A. G. Rozhin, Y. Hsu, Y. Chang, W. Chen, Y. Chen, R. Sankar, F. Chou and C. Liang, *Nanoscale*, 2020, DOI: 10.1039/D0NR01171A.

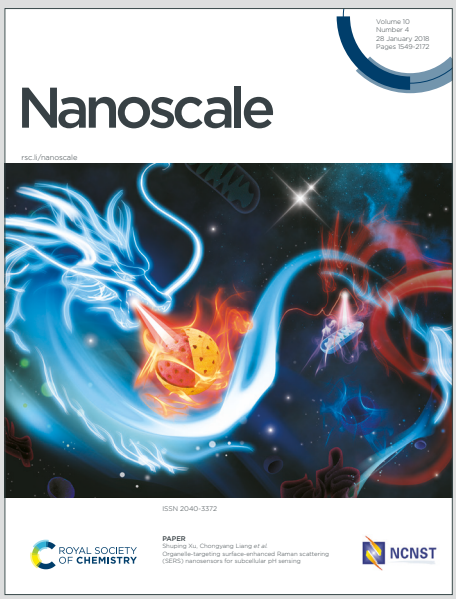

ROYAL SOCIETY OF CHEMISTRY

rsc.li/nanoscale

View Article Online
DOI: 10.1039/D0NR01171A

Unprecedented Random Lasing in 2D Organolead Halide Single-Crystalline Perovskite Microrods

Pradip Kumar Roy†, Rajesh Kumar Ulaganathan†, Raghavan Chinnambedu Murugesan, Swapnil Milind Mhatre, Hung-I Lin, Wei-Liang Chen, Yu-Ming Chang, Alex Rozhin, Yun-Tzu Hsu, Yang-Fang Chen, Raman Sankar, Fang-Cheng Chou* and Chi-Te Liang**

Dr. P. K. Roy, S. M. Mhatre, Y.-T. Hsu, Prof. Y. F. Chen, Prof. C.-T. Liang

Department of Physics, National Taiwan University, Taipei 10617, Taiwan

ctliang@phys.ntu.edu.tw

Dr. R. K. Ulaganathan, Dr. W. L. Chen, Prof. R. Sankar, Prof. Y. M. Chang, Prof. F. C. Chou

Center for Condensed Matter Sciences

National Taiwan University

Taipei 10617, Taiwan

sankarndf@gmail.com, fcchou@ntu.edu.tw

Dr. R. C. Murugesan, Dr. Alex Rozhin

Nanoscience Laboratory, Aston Institute of Photonic Technologies

Aston University

Birmingham B4 7ET, United Kingdom

View Article Online
DOI: 10.1039/D0NR01171A

Prof. R. Sankar

Institute of Physics

Academia Sinica

Taipei 11529, Taiwan

Prof. F. C. Chou

Taiwan Consortium of Emergent Crystalline Materials

Ministry of Science and Technology

Taipei 10622, Taiwan

Prof. F. C. Chou

Center of Atomic Initiative for New Materials

National Taiwan University

Taipei 10617, Taiwan

KEYWORDS: 2D perovskites, Single Crystal, Random laser, 2D quantum-well, low threshold

.

View Article Online
DOI: 10.1039/D0NR01171A

ABSTRACT

Three-dimensional organic-inorganic hybrid halide perovskites have been demonstrated as a great material for applications in optoelectronics and photonics. However, their inherent instabilities over moisture, light, and heat may hinder their road towards the realization of commercialization. Alternatively, emerging two-dimensional (2D) organic-inorganic hybrid perovskites have recently attracted increasing attention owing to their great environmental stability and inherent natural quantum-well structure. In this work, we have synthesized high-quality long-chain organic diammonium spacer assisted 2D hybrid perovskite FA-(N-MPDA)$PbBr_4$ (FA = formamidinium and N-MPDA= N1-methylpropane-1,3-diammonium) by slow evaporation at a constant temperature method. The millimeter-sized single-crystalline microrods demonstrate low-threshold random lasing behavior at room temperature. The single-crystalline 2D hybrid perovskite random laser achieved a very narrow linewidth (~0.1 nm) with a low threshold (~0.5 $\mu J/cm^2$) and a high-quality factor (~5350). Furthermore, the 2D hybrid microrod lasers show stable lasing emission with no measurable degradation after at least 2 h under continuous illumination, which substantially proves the stability of 2D perovskites. Our results demonstrate the promise of 2D organic-inorganic microrod-shaped perovskites and provide an important step toward the realization of high-performance optoelectronic devices.

View Article Online
DOI: 10.1039/D0NR01171A

The Organo-lead halide hybrid perovskites have recently emerged as promising materials due to their wide range of applications in photodetectors, field-effect transistors, solar cells, and a newly added member, random lasers.[1, 2] Typically, organic-inorganic hybrid perovskites are represented by a three-dimensional (3D) lattice framework of ABX_3 (A=MA/FA and B=Pb) chemical formulae. They have excellent light-absorbing characteristics with optically tunable band gaps and have attracted considerable interest especially in the photovoltaic industry for availing solar cell device fabrications due to their low cost and simple large-scale production. Within a short time of their introduction, perovskite solar cells (PSC) have achieved above 20% power conversion efficiency (PCE). But the lack of uniformity, defects in grain boundary/interfacial regions, and poor reproducibility of PSC is a major challenge for obtaining highly stable devices with efficient performances. To overcome these issues, various approaches have been employed, such as introducing super alkali atoms, [3] CdSe quantum dot/PCBM composite as electron transport layer, [4] and passivation using a poly-triarylamine layer. [5] These strategies have expanded the family of PSC. However, these 3D perovskite structures are prone to thermal, moisture, and light-induced degradation, which cause irreversible performance fading. [6-8] In contrast, two-dimensional (2D) organic-inorganic hybrid perovskites are materials with inherent multiple quantum well (QW) structures [9,10], which provide a unique and promising advantage as compared to their 3D counterparts,[11] including both photo-/chemical stability and quantum tunable optoelectronic properties.[12] The 2D perovskites are composed of an inorganic and an organic part. The inorganic perovskite slabs form the 2D conducting layers that are sandwiched between organic barrier layers to form a natural QW structure. The dielectric constant difference between the inorganic and organic layers leads to effective confinement of electron-hole pairs within the QW-like 2D perovskite system, which further inducing excitons with a high binding energy that are stable at

View Article Online
DOI: 10.1039/D0NR01171A

room temperature. Their larger cations hamper interionic motion whereas the organic moieties confer hydrophobicity which increases their moisture tolerance.[13] The properties of perovskites can be tuned easily by changing their 'n' value which essentially gives the number of inorganic layers.[13, 14] Moreover, the value of 'n' determines the width of the QW which leads to strong exciton formation with large binding energy. Compared to polycrystalline thin films, hybrid perovskites in single-crystal form have an advantage of exceptionally long carrier diffusion length because of lower trap densities, improved charge transport, high absorption, and reduced defects due to large grain boundaries. Therefore, it is urgent to search for novel growth methods of preparing single-crystal hybrid perovskites suitable for future optoelectronics.

There are several methods of growing hybrid perovskites reported in the literature, such as slow cooling,[15] inverse temperature crystallization (ITC), [16] and anti-solvent vapor diffusion (ASVD).[17] However, the growth of large-sized single crystals by these techniques is very complicated due to the presence of large organic moieties and long-chain molecules, as well as the possibility of the formation of multi-stacking crystals with random crystallization. In order to overcome these issues, the slow evaporation at constant temperature (SECT) solution growth method has been employed, which efficiently controls the rapid nucleation and reduces the multi-crystallinity of perovskites, to grow millimeter- to centimeter-sized single crystals.[18] Currently, to the best of our knowledge, there is no report on single-crystal growth of N-MPDA based 2D perovskites. To this end, we have focused on the single-crystal growth of (N-MPDA)$PbBr_4$ perovskites with the incorporation of formamidinium (FA) into (N-MPDA)$PbBr_4$ to achieve a stable 2D layered FA-(N-MPDA)$PbBr_4$ perovskite system. Generally, the stability of perovskites depends on the Goldschmidt's tolerance factor (t),[19-21] which is defined as $t = r_A + r_X/\sqrt{2}(r_B+r_X)$. Here, r_A and r_B are the ionic radii of A and B cations, and r_X is the ionic radius of the anion. A

View Article Online
DOI: 10.1039/D0NR01171A

higher value of *t* implies higher stability due to the increased symmetry of the perovskite structure. The tolerance factor of the perovskite is improved by the incorporation of larger ionic molecules into the perovskite lattice which brings several advantages, particularly in maintaining perovskite crystal symmetry and thermal stability. There are many reports which demonstrated the replacement of MA^+ ion by FA^+ ion in order to increase the stability in both single crystals and polycrystalline thin films.[22, 23]

2D perovskites attract a great deal of attention due to their applications in optoelectronics. In a recent report, it has been confirmed that N-MPDA is an excellent candidate for the warm and cold white LEDs due to its broadband emission over the entire visible spectrum. [24] These phenomena propelled our focus to fabricate emerging random laser devices using microrod-shaped FA-(N-MPDA)$PbBr_4$ 2D perovskite single crystals. The random laser exhibits several advantages as compared to conventional laser; which requires a gain medium to amplify light and an optical cavity for the amplification to be efficient. In contrast, a random laser does not require a separate medium, the material itself acts as a gain medium for optical feedback. [25] The gain is provided by the scattering of light which occurs due to the randomness. The light can diffuse and randomly forms closed loops by constructive interference to realize the lasing modes. The major advantage of random lasers lies in its inexpensive and relatively simple technology compared to that of regular lasers. The properties that make a random laser special over regular lasers are its color and angular dependence over the complete solid angle of 4π, which makes it an ideal candidate for display applications. [25] In addition, random lasers have unique characteristics feature of coexistence of the high temporal coherence and low spatial coherence, which makes random lasers an ideal light source for speckle-free imaging. [26] These fascinating phenomena of random lasing can lead to different potential applications, such as super-bright lighting devices, display systems,

View Article Online
DOI: 10.1039/D0NR01171A

Li-Fi, speckle-free imaging technology, *etc*. Our primary motivation is to achieve ultra-low threshold efficient random laser. Several ingredients are necessary to accomplish ultra-low threshold lasing: (i) A high-quality gain medium with slow non-radiative decay pathways at the carrier density levels for population inversion, (ii) High mobilities and free-carrier densities to minimize resistive heat loss, (iii) Good thermal stability, and (iv) A large gain cross-section at the lasing wavelength and sharp band tails. Remarkably, perovskites have exhibited all the aforementioned attributes. Furthermore, utilizing the single-crystalline properties of perovskites, owing to the low trap-state density and long Auger lifetimes, the resultant lasers can demonstrate low lasing thresholds with a very high-quality factor. Recently, 3D hybrid ABX_3 perovskites in the form of thin films, microdisks, nanoplatelets, and quantum dots have been validated as an efficient optical gain media for lasing. [27-32] Nevertheless, room-temperature optical gain and laser behavior from 2D layered perovskites are very rare, which encourages us to explore the possible lasing behavior of 2D FA-(N-MPDA)$PbBr_4$ single crystal.

In this work, we demonstrate room-temperature lasing of 2D perovskite microrods with a low threshold (~0.5 μJ/cm^2), high-quality factors, and excellent photostability in an ambient air environment. The lasing mode linewidth can exhibit an ultra-low value of 0.1 nm and the corresponding quality factor can be as high as 5350, which is highest among single-crystalline perovskites. The remarkable performance of 2D hybrid perovskite microrods can be attributed to a strong absorption coefficient, high-quality factor, 2D quantum confinements, and low non-radiative recombination rates. We believe that our single-crystalline 2D perovskites will pave the way towards the development of solution-based low threshold laser sources.

View Article Online
DOI: 10.1039/D0NR01171A

RESULTS AND DISCUSSION

Figure 1a demonstrates the schematic illustration of the SECT technique for the growth of millimeter size single-crystalline perovskite microrods. This solution growth technique controls the rapid nucleation and reduces the multi-crystalline nature of perovskites to obtain a high-pure phase of single crystals (**Figure S1**). The step-by-step growth process is described as follows. Initially, the saturated solution of FA-(N-MPDA)$PbBr_4$ is prepared by dissolving as-synthesized FA-(N-MPDA)$PbBr_4$ at 120°C (Step 1), under constant magnetic stirring. The saturated solution was stabilized for one hour with continuous stirring to ensure that there are no undissolved minute particles. The solution was then subjected to controlled evaporation in an oil bath at a constant temperature to attain supersaturation (Step 2). During the nucleation process, the excess solute present in the supersaturated solution crystallizes at the bottom (Step 3). We further optimized our saturated solution and allowed a slow evaporation process for 1 day at a constant temperature to attain a high-quality single-crystalline microrod-shaped perovskite. **Figure 1b** displays the optical image of as-synthesized single-crystalline FA-(N-MPDA)$PbBr_4$ microrod, which exhibits a yellowish color. The length and diameter of the crystalline rod are in millimeter and micrometer sizes, respectively (3 mm and 2 μm). The inset of **Figure 1b** shows the top-view SEM image of the as-grown millimeter size perovskite microrod. The X-ray diffraction (XRD) characterization was performed for the as-grown perovskite rods to study the crystal structure and purity (as shown in **Figure 1c, Figure S2**). It shows strong diffraction peaks with regular inter planar spacing at 2θ values of 9.08°, 18.18°, 27.25°, 36.63°, 46.20°, 56.15°, and 66.42°, which are assigned to the (002), (004), (006), (008), (0010), (0012), and (0014) lattice planes, respectively. These diffraction peaks indicate that the surface has a *c*-direction preferred orientation indexed with the (00*l*) planes. The periodic repetitions of the Miller planes reveal the single-crystallinity as well as the layered

View Article Online
DOI: 10.1039/D0NR01171A

behavior of FA-(N-MPDA)$PbBr_4$ perovskites. [31] The lattice parameter values are determined to be a= 12.83, b= 5.94 and c= 13.17 with a space group of P2/m. The as-grown FA-(N-MPDA) $PbBr_4$ microrod crystal was further examined by energy-dispersive X-ray spectroscopy to assess the chemical uniformity. From the EDX mapping (**Figure S3**), the even distribution of C, N, Pb, and Br atoms in the single-crystalline microrod is confirmed. The EDX spectrum of the FA-(N-MPDA)$PbBr_4$ microrod displayed in **Figure S4**, which shows the prominent individual peaks of all atoms. The crystallinity of the FA-(N-MPDA)$PbBr_4$ microrod was investigated by selected area electron diffraction (SAED). The SAED pattern shows the as-grown FA-(N-MPDA)$PbBr_4$ microrod is of good quality and crystallinity in nature (**Figure 1d**). In addition, high resolution transmission electron microscopy (HR-TEM) was performed as shown in **Figure 1e**, which confirms the spacing between the lattice fringes is about 0.25 nm. Photoluminescence (PL) experiments were performed to characterize the optical properties and to understand the uniformity of the single crystals. The microrods were transferred to a clean glass plate substrate and excited by an 8-MHz 405 nm pulsed laser. The PL measurements were carried out with a 10x objective and 3 μW power irradiation on the sample. **Figure 2a** shows the typical emission spectrum with the emission peak centered at 535 nm. The PMT mapping image of a microrod is shown in **Figure 2b**. The PL spectral mapping was conducted over the rectangular marked area. The emission peak center of the spectral mapping illustrates in **Figure 2c**, where different colors represent the peak center values of the mapping area. It is found that the emission peak centers are uniformly distributed over the crystal, confirming the as grown FA-(N-MPDA) $PbBr_4$ microrods are of good quality.[18, 33] The histogram of the emission peak demonstrates a distribution that centers at ~535 nm (**Figure 2d**). The sharp spectrum reveals the excellent optical quality of the single-crystalline microrod.[18]

View Article Online
DOI: 10.1039/D0NR01171A

The schematic illustration of the generation of random lasers via 2D perovskite single crystal is depicted in **Figure 3a**. Although we have a single-crystalline perovskite microrod as evidenced by the XRD results, it is inevitable that there exist some defects and dislocations in our large-size (3 mm x 2 □m) sample. These crystal imperfections, together with the surfaces of our single-crystal microrod that can be considered as the grain boundaries, behave as scattering centers, where the spontaneously emitted photons are scattered in all directions. Some Fabry- Pérot-like peaks (when light bounces back and forth along the crystal) may well co-exist with the random lasing ones. After multiple scattering, the closed loops are formed inside the optical gain media and provide coherent feedback via constructive interference to the emission.[34] As a result, laser action is achieved. As shown in **Figure 3b and Figure S5**, multiple sharp lasing peaks have been observed, even for spectrally close lasing modes. This can be attributed to the fact that the lasing modes overlap very weakly due to their exponential confinement.[35] Due to a large refractive index contrast at the end facets between the organic-inorganic hybrid single-crystalline perovskite rod and its outside environment, [36] which itself can act as a gain medium, leading to the very small critical angle for total internal reflection inside the crystal. This fascinating feature enhanced the light-trapping probability inside the crystal, which may ensure a further enhancement at the internal light scattering.

The random lasing action was studied under an excitation of 374 nm pulsed laser of the frequency of 40 MHz and a pulse width of 55 ps. **Figure 3b** shows the evolution of PL spectra as a function of pumping energy density. At low pumping energies, the PL spectra show a broad emission profile with a nearly Gaussian shape and a higher full width at half maximum (FWHM) of ~25 nm (**Figure S6**). When the incident power exceeds the threshold (P_{th}), the spectra start showing sharp

View Article Online
DOI: 10.1039/D0NR01171A

emission peaks, which reveals the transition from spontaneous emission to stimulated emission. It is worth mentioning that, multiple sharp peaks of the random laser can be seen throughout the whole spectrum, which might be quite interesting for display application. The multiple peaks in the spectra signify the number of modes with interference providing substantial feedback. The FWHM ($\delta\lambda$) of individual lasing peaks of the dominating lasing mode is as low as ~0.1 nm (fitted by a Gaussian function, **Figure S7**), which gave rise to a high cavity quality factor of ~5350 (at 535 nm emission wavelength) calculated by using the relationship $Q = \lambda/\delta\lambda$ (Supporting Information). As a side note, the most important characteristics of a laser device, the spectra coherence, can be evaluated by lasing linewidth. As described by the Schawlow-Townes equation, the lasing linewidth is constrained by *Q* factor and gain value of semiconductor, and the coupling efficiency of spontaneous emission into the lasing process.[37] The spectral linewidth and intensity vs the pumping energy density can be seen in **Figure 3c**. The threshold value of pumping energy density is as low as 0.5 $\mu J/cm^2$. Beyond the threshold value, we can see that the FWHM decreases drastically from 25 nm to 0.1 nm. The narrowing of emission peak in the spectra is proof of prominent lasing action. The low threshold of the random laser can be attributed to the large exciton binding energies (~300 meV (Figure S8)) [13] of 2D hybrid single-crystalline rod and the scattered light, which may form coherent feedback loops inside the 2D single crystal. The threshold value for a random laser is known to be inversely proportional to the mean free path of the emitted photons. Owing to the highly crystalline nature and low trap state density, the 2D single crystals are known to have a long mean free path and hence a very low lasing threshold.[38] Besides, it is reported that to attain a lower pumping threshold energy value, the Auger recombination should be much slower. [39, 40] The single-crystal structure exhibits much slower Auger

View Article Online
DOI: 10.1039/D0NR01171A

recombination compared to that of colloidal perovskites, which helps to decrease the lasing threshold.

To verify the characteristic of the random lasing action, we conducted angle-dependent PL measurements and area dependence of the emission spectra. **Figure 4a** displays the emission spectra from different angles ranging from -20° to +20°, where the collection angles are achieved by vertically rotating the sample with respect to the line of incidence of the pumping laser as shown in the insets of **Figure 4a**. Quite interestingly, the achieved spectra show lasing phenomena in each measured angle, which provides firm evidence of the random lasing behavior and confirms the multi-directionality of the random laser output. The localization of light is not always in the same direction or the same path, hence different localization paths will result in random laser with different directions. It is important to mention that the number of laser modes for both rotation angles (-20° and +20°) decreases compared to a 0° rotation. This phenomenon is expected, as the tiling of the sample changes random media in terms of gain. Due to this reason, the modes will be different.[41] We have measured the laser spectra with different objective lenses to study the dependence of emitted spectra on pumping laser spot size with a fixed incident energy density of 12 μJ/cm^2 as shown in **Figure 4b and Figure S9**. We collected the emission spectra by different objective lenses, 60X and 100X corresponding to an illumination area of 23.80 and 12.56 μm^2 respectively. These results show that with the increase of excitation area, the lasing peaks are found to be stronger as it can form more closed-loop paths for the emitted photons in a larger excitation volume.[42] Alternatively, the number of modes collected by 100X lens in **Figure 3b** is increased with increasing pumping energy density as the saturation of the number of modes has not been obtained. [43] The random laser model fits quite well with the observed emitted spectra.

View Article Online
DOI: 10.1039/D0NR01171A

The ambient stability of random laser devices is one of the essential parameters for its practical applications. In order to prove the ambient stability of our devices, we have recorded the emission spectra and microscopy image of our random laser device with time as shown in **figure 5**. **Figure 5a** shows that the shape and intensity of microscope images remain unchanged with time. The intensity of the laser spectrum remained stable over for more than two hours in ambient conditions as shown in **Figure 5b**, which attested the stability of our 2D perovskites. In short, the multiple time's observation of the laser action from a single point of the device resembles the stable lasing action from the device,[44] which can be attributed to the stable and fascinating optical properties of 2D single-crystalline perovskites.

In order to further demonstrate the dynamic process of the lasing action, we performed time-resolved photoluminescence (TRPL) under different pumping energy density of the same excitation source. The TRPL decay curves at different excitation fluences spanning from PL to random lasing processes are illustrated in **Figure 6a**. We further plot the obtained excited state carrier lifetime as a function of pumping energy density in **Figure 6b**. At lower pumping energy fluences (less than the threshold), the decay profile fitted by an exponential function yields a lifetime of ~4.5 ns, whereas a very fast decay time of ~0.12 ns is obtained when the excitation fluence is above the threshold. This phenomenon indicates the occurrence of a stimulated emission process and lasing action in the 2D perovskites device (**Figure 3b**). Such a low lifetime can be attributed to a higher recombination rate as there are a larger number of modes available. It is well known that the radiation density is directly proportional to the recombination rate in the matrix,

View Article Online
DOI: 10.1039/D0NR01171A

due to this reason the abrupt decrease of carrier lifetime at the threshold pumping energy signifies the stimulated emission process and provides strong evidence of lasing occurrence.[44, 45]

CONCLUSION

We have successfully grown millimeter-sized high-quality 2D single-crystal perovskite (FA-(N-MPDA)$PbBr_4$) using the SECT solution growth technique. The 2D hybrid single crystal exhibits a high crystallinity with a well-defined rod-shaped structure, resulting in good optical properties with a uniform emission center at 535 nm over an entire region. The random lasing properties of 2D single-crystal perovskite have been investigated with long-term stability over 2 hours under ambient atmosphere. To the best of our knowledge, this is the first attempt of designing a laser device based on single-crystalline FA-(N-MPDA)$PbBr_4$ microrod structure, which demonstrates a robust reduction of laser threshold (0.5 μJ/ cm^2) with a highly narrow lasing linewidth (0.1 nm) and superior quality factor of 5350 (at 535 nm emission wavelength). The low threshold can be attributed to the strong quantum confinement, long mean free path, and large exciton binding energy of the 2D single-crystal perovskite. The unprecedented and versatile optical performance together with its 2D single-crystalline structure may hold the key to realizing solution-processed random lasing for future optoelectronic exploration and development.

Experimental Section

Preparation of precursor material & Single-crystal growth of FA-(N-MPDA)$PbBr_4$: For the preparation of precursor material, the raw materials Lead oxide (PbO), Hydrobromic acid (HBr),

View Article Online
DOI: 10.1039/D0NR01171A

N1-methylpropane-1,3-diammonium ($CH_3NH(CH_2)_3NH_2$) (N-MPDA), and *Formamidinium* chloride ($HC(NH_2)_2Cl$) were used. All the chemicals with high purity were purchased from Sigma Aldrich. Initially, PbO (10 mmol) was dissolved in HBr at 70° C under continuous stirring until the formation of a clear bright yellow solution. In parallel, $CH_3NH(CH_2)_3NH_2$ (3.33 mmol) was added dropwise into an HBr solution with continuous stirring to form $(N\text{-}MPDA)^+Br^-$ salt solution. The above neutralization reaction is exothermic; therefore, it was carried out in an ice bath. To obtain the 2D $(N\text{-}MPDA)PbBr_4$ perovskite, the neutralized cold salt solution of $(N\text{-}MPDA)^+Br^-$ was added into the hot PbO solution at 120° C. Yellow precipitation will start to occur, which must be redissolved by continuous stirring followed by the addition of slightly excessive HBr solution to get a clear bright yellow solution. The final solution is allowed to rest for slow evaporation at a constant temperature to obtain an $(N\text{-}MPDA)PbBr_4$ perovskite compound. For the synthesis of FA-$(N\text{-}MPDA)PbBr_4$ perovskite material, FACl was added into the PbO solution first, followed by the dropwise addition of $(N\text{-}MPDA)^+Br^-$ solution with continuous stirring. To obtain a millimeter-sized crystal, we followed the SECT growth technique in which the supersaturated solution was allowed for slow evaporation at a constant temperature over 1 day. During the nucleation, the excess solute in the supersaturated solution starts to crystallize at the bottom of the beaker in a larger size.

Characterizations: XRD pattern was obtained from Bruker D2 PHASER (CuKα radiation). The scanning electron microscopy (SEM) and energy-dispersive X-ray spectroscopy (EDX) mapping were performed by (FEI, Nova 200) to analyze the morphology and chemical constituents of the FA-$(N\text{-}MPDA)PbBr_4$ perovskite single crystal. A pulsed laser of wavelength 374 nm was used as the pumping source for studying the lasing spectra and carrier lifetime. A Horiba–Jobin–Yvon TRIAX 320 spectrometer was used as a signal collector with 100x objective. The laser incident

View Article Online
DOI: 10.1039/D0NR01171A

area dependent lasing spectra were acquired using a Horiba–Jobin–Yvon TRIAX 320 spectrometer with 60x (LMPlanFI, Japan) and 100x (Olympus, Japan) objectives.

SUPPORTING INFORMATION

Supporting Information is available from the Wiley Online Library or from the authors and contains a brief description of the SECT growth method, EDX analysis, below threshold PL emissions, Tauc plot with binding energy calculations, and Q-Factor Calculations.

AUTHOR INFORMATION

Corresponding Authors

ctliang@phys.ntu.edu.tw, sankarndf@gmail.com, and fcchou@ntu.edu.tw

Author Contributions

The manuscript was written through contributions of all authors. All authors have given approval to the final version of the manuscript.

† PKR and RKU contributed equally.

Funding Sources

The work was supported by the Ministry of Science and Technology and Ministry of Education of the Republic of China

View Article Online
DOI: 10.1039/D0NR01171A

REFERENCES

(1) X. Gao, X. Zhang, W. Yin, H. Wang, Y. Hu, Q. Zhang, Z. Shi, V. L. Colvin, W. W. Yu, Y. Zhang, *Adv. Sci.* **2019**, *6*, 1900941

(2) M. Liu, H. Zhang, D. Gedamu, P. Fourmont, H. Rekola, A. Hiltunen, S. G. Cloutier, R. Nechache, A. Priimagi, P. Vivo, *Small* **2019**, *15*, 1900801.

(3) M. Wang, H. Wang, W. Li, X. Hu, K. Sun, Z. Zang, *J. Mater. Chem. A* **2019**, 7, 26421-26428.

(4) X. Zeng, T. Zhou, C. Leng, Z. Zang, M. Wang, W. Hu, X. Tang, S. Lu, L. Fang, M. Zhou, *J. Mater. Chem. A* **2017**, 5, 17499.

(5) T. Zhou, M. Wang, Z. Zang, L. Fang, *Adv. Energy Mater.* **2019**, 9, 1900664.

(6) I. C. Smith, E. T. Hoke, D. Solis-Ibarra, M. D. McGehee, H. I.Karunadasa, *Angew. Chem. Int. Ed.* **2014,** *53*, 11232.

(7) D. H. Cao, C. C Stoumpos, O. K. Farha, J. T. Hupp, M. G. Kanatzidis, *J. Am. Chem. Soc.* **2015,** *137* , 7843.

(8) C. Ma, C. Leng, Y. Ji, X. Wei, K. Sun, L. Tang, J. Yang, W. Luo, C. Li, Y. Deng, S. Feng, J. Shen, S. Lu, C. Du, H. Shi, *Nanoscale* **2016,** *8*, 18309.

(9) T. Zhou, M. Wang, Z. Zang, X. Tang, L. Fang, *Sol. Energy Mater. Sol. Cells* **2019**, 191, 33.

(10) H. Tsai, W. Nie, J.-C. Blancon, C. C. Stoumpos, R. Asadpour, B. Harutyunyan , A. J. Neukirch, R. Verduzco, J. J. Crochet, S. Tretiak, L. Pedesseau, J. Even, M. A. Alam, G. Gupta, J. Lou, P. M. Ajayan, M. J. Bedzyk, M. G. Kanatzidis, A. D. Mohite, *Nature* **2016**, *536*, 312.

(11) J. Chen, Y. Wang, L. Gan, Y. He, H. Li, T. Zhai, *Angew. Chem. Int. Ed.* **2017**, *56*, 14893.

(12) C. R. Kagan, D. B. Mitzi, C. D. Dimitrakopoulos, *Science* **1999**, *286*, 945.

View Article Online
DOI: 10.1039/D0NR01171A

(13) J.-C. Blancon, H. Tsai, W. Nie, C. C. Stoumpos, L. Pedesseau, C. Katan, M. Kepenekian, C. M. M. Soe, K. Appavoo, M. Y. Sfeir, S. Tretiak, P. M. Ajayan, M. G. Kanatzidis, J. Even, J. J. Crochet, A. D. Mohite, *Science* **2017**, *355*, 1288.

(14) C. C. Stoumpos, D. H. Cao, D. J. Clark, J. Young, J. M. Rondinelli, J. I. Jang, J. T. Hupp, M. G. Kanatzidis, *Chem. Mater.* **2016**, *28*, 2852.

(15) W. Peng, J. Yin, K.-T. Ho, O. Ouellette, M. De Bastiani, B. Murali, O. El Tall, C. Shen, X. Miao, J. Pan, E. Alarousu, J.-H. He, B. S. Ooi, O. F. Mohammed, E. Sargent, O. M. Bakr, *Nano Lett.* **2017**, *17*, 4759.

(16) G. Maculan, A. D. Sheikh, A. L. Abdelhady, M. I. Saidaminov, M. A. Haque, B. Murali, E. Alarousu, O. F. Mohammed, T. Wu, O. M. Bakr, *J. Phys. Chem. Lett.* **2015**, *6*, 3781.

(17) D. Shi, V. Adinolfi, R. Comin, M. Yuan, E. Alarousu, A. Buin, Y. Chen, S. Hoogland, A. Rothenberger, K. Katsiev, Y. Losovyj, X. Zhang, P. A. Dowben, O. F. Mohammed, E. H. Sargent, O. M. Bakr, *Nano Lett.* **2015**, *347*, 519.

(18) C. M. Raghavan, T.-P. Chen, S.-S. Li, W.-L. Chen, C.-Y. Lo, Y.-M. Liao, G. Haider, C.-C. Lin, C.-C. Chen, R. Sankar, Y.-M. Chang, F.-C. Chou, C.-W. Chen, *Nano Lett.* **2018**, *18*, 3221.

(19) C. J. Bartel, C. Sutton, B. R. Goldsmith, R. Ouyang, C. B. Musgrave, L. M. Ghiringhelli, M. Scheffler, *Sci. Adv.* **2019**, 5, 0693.

(20) G. Kieslich, S. Sun, A. K. Cheetham, *Chem. Sci.* **2014**, *5*, 4712.

(21) Z. Li, M. Yang, J.-S. Park, S.-H. Wei, J. J. Berry, K. Zhu, *Chem. Mater.* **2016**, *28*, 284.

(22) Q. Han, S.-H. Bae, P. Sun, Y.-T. Hsieh, Y. Yang, Y. S. Rim, H. Zhao, Q. Chen, W. Shi, G. Li, Y. Yang, *Adv. Mater.* **2016**, *28*, 2253.

View Article Online
DOI: 10.1039/D0NR01171A

(23) T. Niu, J. Lu, M.-C. Tang, D. Barrit, D.-M. Smilgies, Z. Yang, J. Li, Y. Fan, T. Luo, I. McCulloch, A. Amassian, S. Liu, K. Zhao, *Energy Environ. Sci.* **2018**, *11*, 3358.

(24) E. R. Dohner, E. T. Hoke, H. I. Karunadasa, *J. Am. Chem. Soc.* **2014**, *136*, 1718.

(25) D. S. Wiersma, *Nat. Phys.* **2008**, *4*, 359.

(26) B. Redding, M. A. Choma, H. Cao, *Nat. Photonics* **2012**, *6*, 355.

(27) Q. Zhang, R. Su, X. Liu, J. Xing, T. C. Sum, Q. Xiong, *Adv. Func. Mater.* **2016**, *26*, 6238.

(28) G. Xing, N. Mathews, S. S. Lim, N. Yantara, X. Liu, D. Sabba, M. Grätzel, S. Mhaisalkar, T. C. Sum, *Nat. Mater.* **2014**, *13*, 476.

(29) Q. Liao, K. Hu, H. Zhang, X. Wang, J. Yao, H. Fu, *Adv. Mater.* **2015**, *27*, 3405.

(30) P. K. Roy, G. Haider, H.-I. Lin, Y.-M. Liao, C.-H. Lu, K.-H. Chen, L.-C. Chen, W.-H. Shih, C.-T. Liang, Y.-F. Chen, *Adv. Opt. Mater.* **2018**, *6*, 1800382.

(31) Y. Hu, L. M. Spies, D. Alonso-Álvarez, P. Mocherla, H. Jones, J. Hanisch, T. Bein, P. R. F. Barnes, P. Docampo, *J. Mater. Chem. A* **2018**, *6*, 22215.

(32) M. Anni, D. Rhee, W.-K. Lee, *ACS Appl. Mater. Interfaces.* **2019**, *11*, 9385.

(33) J. Wang, J. Li, S. Lan, C. Fang, H. Shen, Q. Xiong, D. Li, *ACS Nano* **2019**, *13*, 5473.

(34) M. L. De Giorgi, M. Anni, *Appl. Sci.* **2019,** *9* , 4591.

(35) P. Stano, P. Jacquod, *Nat. Photonics.* **2013**, *7*, 66.

(36) B. Liu, C. M. M. Soe, C. C. Stoumpos, W. Nie, H. Tsai, K. Lim, A. D. Mohite, M. G. Kanatzidis, T. J. Marks, K. D. Singer, *Sol. RRL* **2017**, *1*, 1700062.

View Article Online
DOI: 10.1039/D0NR01171A

(37) A. L. Schawlow, C. H. Townes, *Phys. Rev.* **1958**, *112*, 1940.

(38) H. Zhu, Y. Fu, F. Meng, X. Wu, Z. Gong, Q. Ding, M. V. Gustafsson, M. T. Trinh, S. Jin, X. Y. Zhu, *Nat. Mater.* **2015**, *14*, 636.

(39) S. A. Veldhuis, P. P. Boix, N. Yantara, M. Li, T. C. Sum, N.Mathews, S. G. Mhaisalkar, *Adv. Mater.* **2016,** *28*, 6804.

(40) B. R. Sutherland, E. H. Sargent, *Nat. Photonics* **2016**, *10*, 295.

(41) J. Liu, P. D. Garcia, S. Ek, N. Gregersen, T. Suhr, M. Schubert, J. Mørk, S. Stobbe, P. Lodahl, *Nat. Nanotechnol.* **2014**, 9, 285.

(42) Y. Ling, H. Cao, A. L. Burin, M. A. Ratner, X. Liu, R. P. H. Chang, *Phys. Rev. A* **2001**, *64*, 063808.

(43) H. Cao, Y. G. Zhao, S. T. Ho, E. W. Seelig, Q. H. Wang, R. P. H. Chang, *Phys. Rev. Lett.* **1999**, *82*, 2278.

(44) H.-W. Hu, G. Haider, Y.-M. Liao, P. K. Roy, R. Ravindranath, H.-T. Chang, C.-H. Lu, C.-Y. Tseng, T.-Y. Lin, W.-H. Shih, Y.-F. Chen, *Adv. Mater.* **2017**, *29*, 1703549.

(45) G. Haider, R. Ravindranath, T.-P. Chen, P. Roy, P. K. Roy, S.-Y. Cai, H.-T. Chang, Y.-F. Chen, *Nat. Commun.* **2017**, *8*, 256.

View Article Online
DOI: 10.1039/D0NR01171A

Figures and figure captions:

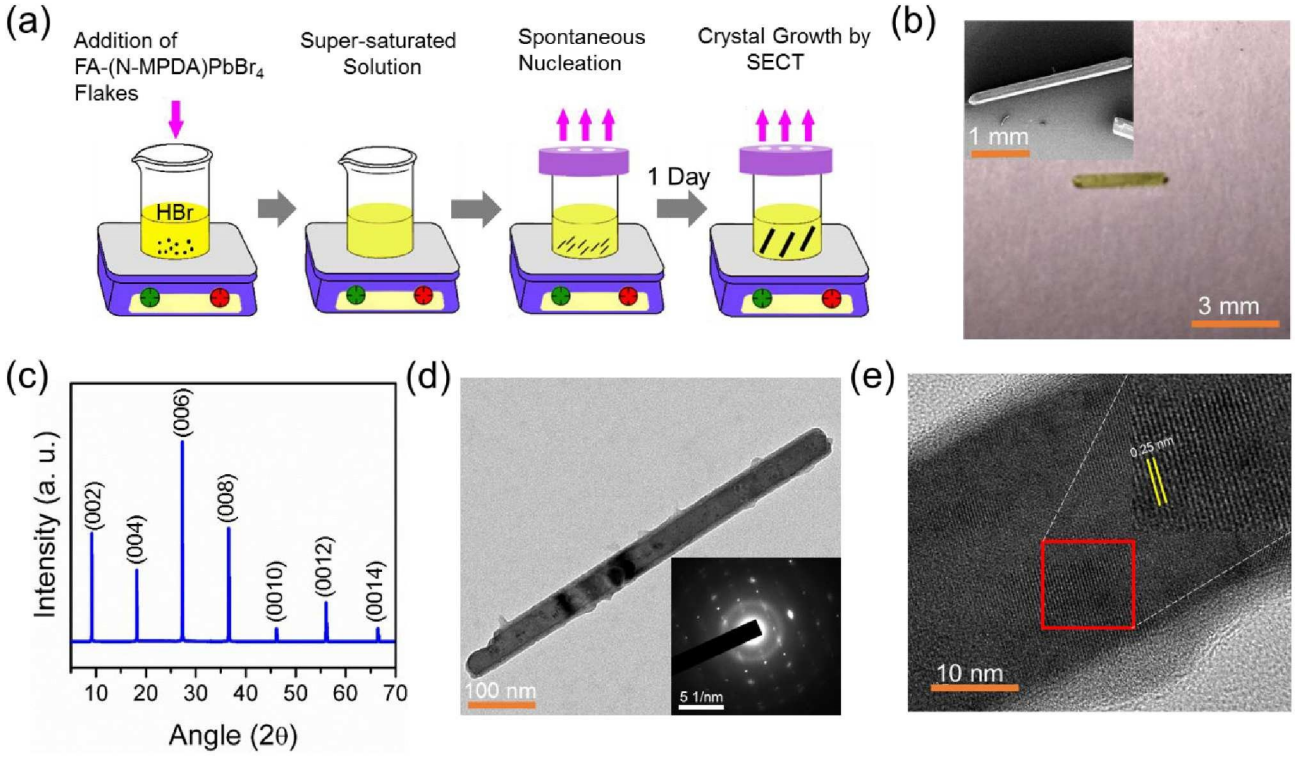

Figure 1. (a) Schematic illustration of the synthesis of FA-(N-MPDA)$PbBr_4$ microrod. (b) Optical image of the as-synthesized microrod ~ 3 mm in length. (Inset: Top-view SEM image of the microrod) (c) XRD pattern of 2D microrod (d) TEM Image of FA-(N-MPDA)$PbBr_4$ microrod at lower magnification with the SAED pattern (Inset). (e) HR-TEM of FA-(N-MPDA)$PbBr_4$ microrod is displayed with the lattice fringes of about 0.25 nm.

View Article Online
DOI: 10.1039/D0NR01171A

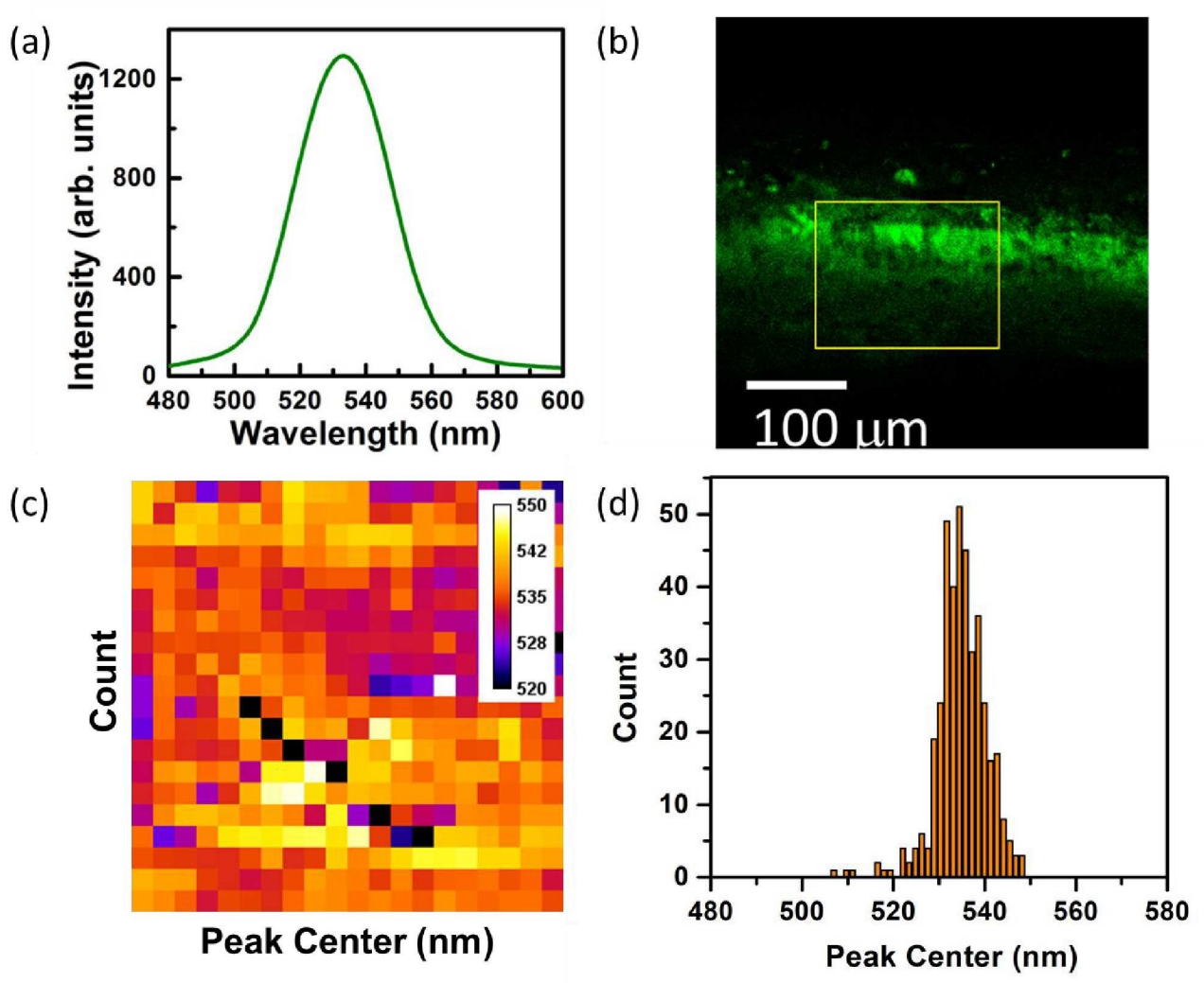

Figure 2. (a) The emission peak of as synthesized microrod with a peak centered at 535 nm. (b) PMT mapping of a microrod with the yellow rectangle showing the area used for spectral mapping. (c & d) Peak center mapping and the corresponding histogram distribution of the yellow rectangular area shown in (b). The mapping confirms the microrod uniformity.

View Article Online
DOI: 10.1039/D0NR01171A

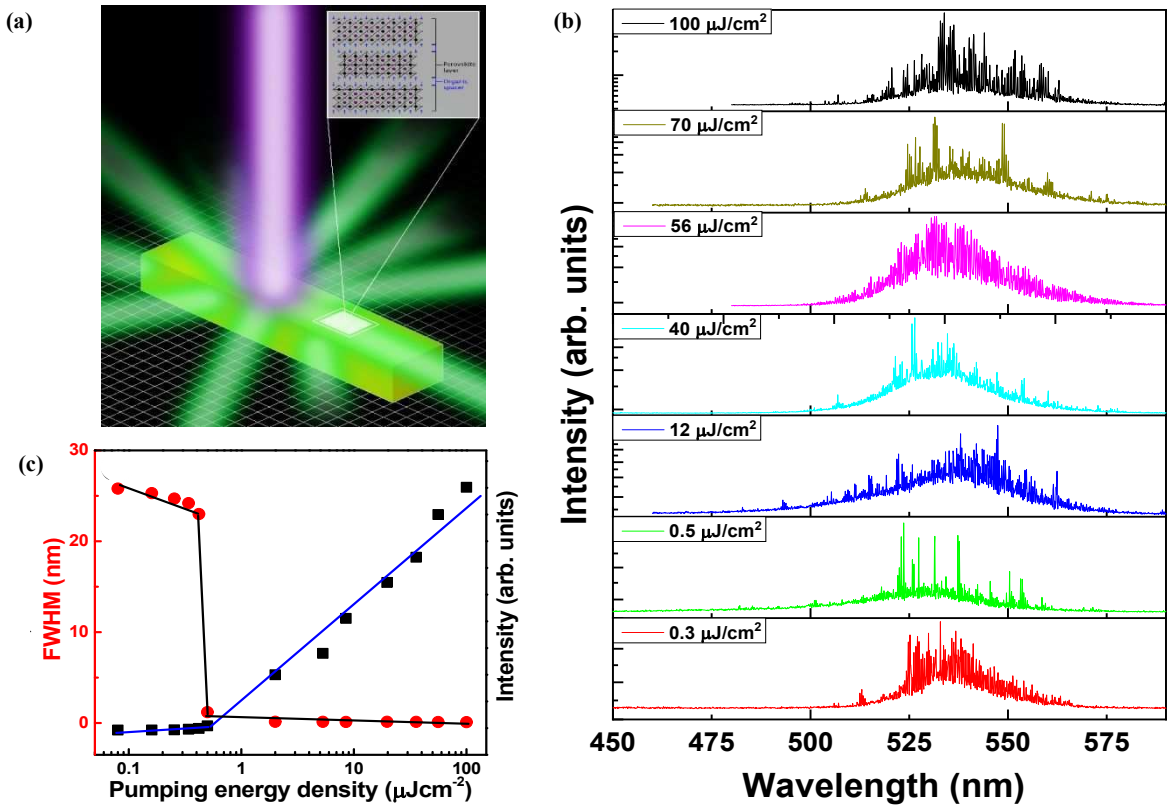

Figure 3: (a) Schematic illustration of random lasers in single-crystalline 2D perovskite microrod. The enlarged picture illustrates the multiple quantum walls structures formation formed by the organic and inorganic molecules in 2D perovskite. (b) Random lasing from 2D perovskite single crystal microrod on a semi-log scale. Evolution of the emission spectra of 2D perovskite device as a function of pumping energy density. (c) Integrated intensities and emission line widths as a function of pump fluence. A prominent linewidth narrowing occurs near the threshold of P_{th} = 0.5 μJ/cm^2, accompanied by a sharp increase of emission intensity.

View Article Online
DOI: 10.1039/D0NR01171A

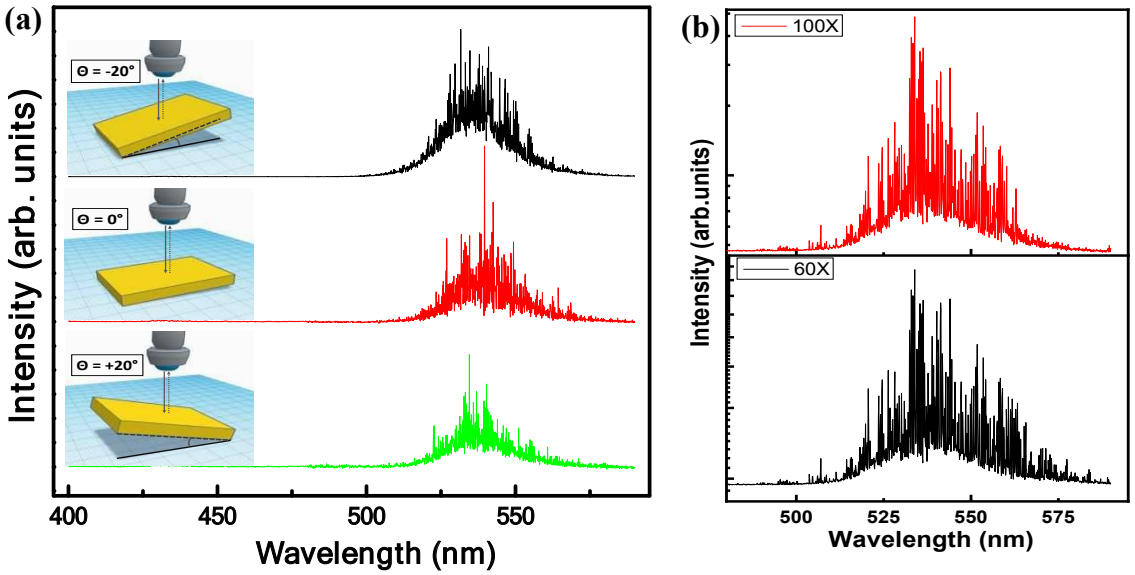

Figure 4. Evidence of random lasing from 2D perovskite single-crystalline microrod. (a) Angular dependence of lasing emission spectra noted at a constant pump fluence of 12 μJ/ cm^2. The angles +20, 0, and −20 degrees are achieved by vertically rotating the sample with respect to the line of incidence of the pumping laser as shown in the insets of the respective spectrum. The lines serve as a guide to the eye. (b) Variation of the laser spot size of the emitted spectrum on a semi-log scale while keeping the power density fixed at 12 μJ/ cm^2.

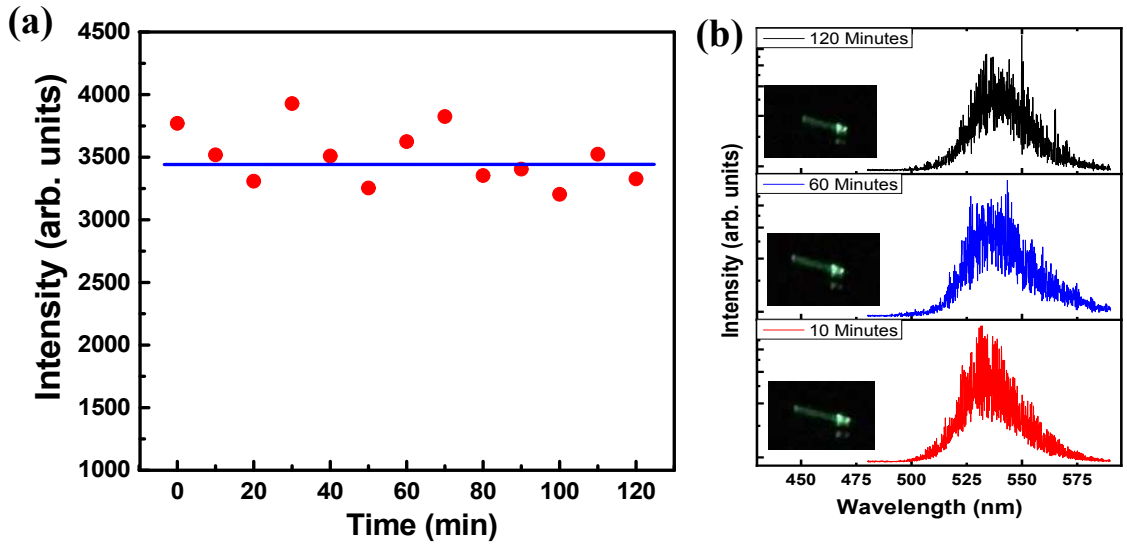

Figure 5. Random lasing stability measurements of 2D perovskite single-crystalline microrod. (a) Lasing (centered at ~535 nm) under pumping at 374 nm with a fluence 12 μJ/cm^2 with time. (b) Random lasing spectra and microscopy image recorded at a constant pump fluence of 12 μJ/cm^2 as a function of time.

View Article Online
DOI: 10.1039/D0NR01171A

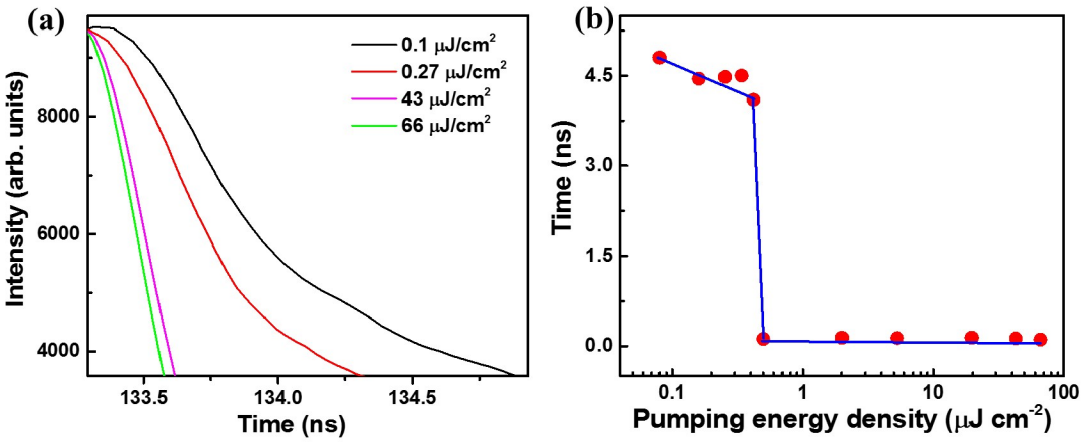

Figure 6. Lifetime measurements of 2D perovskite single-crystalline microrod. (a) Typical PL dynamics obtained at different pumping energy densities. (b) Calculated excited state carrier lifetime as a function of pumping energy density. A prominent lifetime change occurs near the threshold of P_{th} = 0.5 μJ/cm².

View Article Online
DOI: 10.1039/D0NR01171A

For Table of Contents Only

Low threshold random lasing phenomena from a millimeter-sized 2D single-crystalline perovskite (FA-(N-MPDA)$PbBr_4$) microrod. The lower value of the threshold can be attributed to the strong light confinement, long mean free path and large exciton binding energy in the 2D layered perovskite structure.

Keywords: 2D perovskites, Single crystal, Random laser, 2D quantum-well, Low threshold

Pradip Kumar Roy†, Rajesh Kumar Ulaganathan†, Raghavan Chinnambedu Murugesan, Swapnil Milind Mhatre, Hung-I Lin, Wei-Liang Chen, Yu-Ming Chang, Alex Rozhin, Yun-Tzu Hsu, Yang-Fang Chen, Raman Sankar, Fang-Cheng Chou* and Chi-Te Liang**

Unprecedented Random Lasing in 2D Organolead Halide Single-Crystalline Perovskite Microrods